Draft version July 20, 2010
Preprint typeset using LaTeX style emulateapj v. 12/01/06

FALLBACK SUPERNOVAE: A POSSIBLE ORIGIN OF PECULIAR SUPERNOVAE WITH EXTREMELY LOW EXPLOSION ENERGIES

Takashi Moriya[1,2,3], Nozomu Tominaga[4,1], Masaomi Tanaka[1], Ken'ichi Nomoto[1,2], Daniel N. Sauer[5], Paolo A. Mazzali[6,7,8], Keiichi Maeda[1], and Tomoharu Suzuki[2]

Draft version July 20, 2010

ABSTRACT

We perform hydrodynamical calculations of core-collapse supernovae (SNe) with low explosion energies. These SNe do not have enough energy to eject the whole progenitor and most of the progenitor falls back to the central remnant. We show that such fallback SNe can have a variety of light curves (LCs) but their photospheric velocities can only have some limited values with lower limits. We also perform calculations of nucleosynthesis and LCs of several fallback SN model, and find that a fallback SN from the progenitor with a main-sequence mass of 13 $M_\odot$ can account for the properties of the peculiar Type Ia supernova SN 2008ha. The kinetic energy and ejecta mass of the model are 1.2×10^{48} erg and 0.074 $M_\odot$, respectively, and the ejected ^{56}Ni mass is 0.003 $M_\odot$. Thus, SN 2008ha can be a core-collapse SN with a large amount of fallback. We also suggest that SN 2008ha could have been accompanied with long gamma-ray bursts and long gamma-ray bursts without associated SNe may be accompanied with very faint SNe with significant amount of fallback which are similar to SN 2008ha.

Subject headings: gamma-ray burst: general – supernovae: general – supernovae: individual (SN 2008ha)

1. INTRODUCTION

A massive star with main-sequence mass above ~ 10 $M_\odot$ is thought to end its life as a supernova (SN) after forming an Fe core at its center. The SN is triggered by the gravitational collapse of the Fe core, thus being called a core-collapse SN. The mechanism that leads to the final emergence of an SN from the collapse is still under debate but observations show that ejecta of the SN normally has a kinetic energy of $\sim 10^{51}$ erg. Currently, however, theoretical attempts to simulate the whole explosion of a core-collapse SN have not obtained explosion energy as large as 10^{51} erg (see, e.g., Janka et al. 2007; Bruenn et al. 2009; Burrows et al. 2007; Suwa et al. 2009).

If the explosion energy is low, the inner part of the star falls back onto the central remnant and only the outer part of the star overcomes the gravitational potential. The idea of the fallback was first introduced by Colgate (1971) and many studies have since investigated the effects of the fallback onto the central remnant, e.g., black hole formation (*e.g.,* Chevalier 1989; Woosley & Weaver 1995; Fryer 1999; MacFadyen et al. 2001; Zhang et al. 2008). Recently, more attention has been paid to the outer part, which eventually escapes from fallback, thus being ejected. The ejecta might be observed as an SN (*e.g.,* Fryer et al. 2007, 2009) and could produce the peculiar chemical abundance patterns of extremely metal-poor stars (*e.g.,* Iwamoto et al. 2005). As this ejecta has a kinetic energy just above the value required to overcome the gravitational potential, it is expected to have very low energy. If enough amount of ^{56}Ni is also ejected or the ejecta interacts with the circumstellar medium (Fryer et al. 2009), this ejecta might be observed as an SN having very low line velocities.

In this connection, the peculiar SN 2008ha is a suitable object, with sufficient observational data that can be compared with the fallback SN models. SN 2008ha was discovered on 2008 November UT 7.17 (Puckett, Moore, Newton, & Orff 2008) and was found to be one of the faintest SNe ever discovered (Valenti et al. 2009, hereafter V09; Foley et al. 2009, hereafter F09). It was found in an irregular galaxy UGC 12682 at a distance modulus of $\mu = 31.64$ mag (F09). Adopting a galactic extinction of $E(B-V) = 0.08$ mag and little host extinction, the peak absolute V-band magnitude was found to be as faint as -14.21 ± 0.15 mag (F09). From its spectral similarities to SN 2002cx-like Type Ia SNe, SN 2008ha was classified as a peculiar Type Ia SN.

SN 2002cx-like SNe make a class of peculiar Type Ia SNe (see, e.g., the supplementary information of V09; SN 2002cx (Li et al. 2003; Jha et al. 2006) and SN 2005hk (Phillips et al. 2007; Sahu et al. 2008) are well-studied examples of this class). Their spectra do not have strong absorptions of Si and S at early epochs [9], which are the characteristic features of normal Type Ia SNe. Line velocities of SN 2002cx-like SNe are very low compared with normal Type Ia SNe (Branch et al. 2004). They also have peculiar light curves (LCs), which decline slowly in spite of their low maximum luminosities and do

[1] Institute for the Physics and Mathematics of the Universe, University of Tokyo, Kashiwanoha 5-1-5, Kashiwa, Chiba 277-8583, Japan; takashi.moriya@ipmu.jp
[2] Department of Astronomy, Graduate School of Science, University of Tokyo, Bunkyo-ku, Tokyo 113-0033, Japan
[3] Research Center for the Early Universe, Graduate School of Science, University of Tokyo, Bunkyo-ku, Tokyo 113-0033, Japan
[4] Department of Physics, Faculty of Science and Engineering, Konan University, 8-9-1 Okamoto, Kobe, Hyogo 658-8501, Japan
[5] Department of Astronomy, Stockholm University, Albanova University Center, SE-106 91 Stockholm, Sweden
[6] Max Planck Institute for Astrophysics, Karl-Schwarzschild-Straße 1, 85741 Garching, Germany
[7] Scuola Normale Superiore, Piazza dei Cavalieri, 7, 56126 Pisa, Italy
[8] INAF-OAPd, vicolo dell'Osservatorio, 5, 35122 Padova, Italy

[9] However, the earliest observed spectrum of SN 2008ha before the maximum luminosity showed these features (Foley et al. 2010), although these features disappeared soon (V09; F09).

not show a second peak which appears in the I and R band LCs of normal Type Ia SNe.

SN 2008ha has additional peculiarities. The rise time of SN 2008ha is faster than that of normal Type Ia SNe and the decline of the LC after the maximum is very rapid: $\Delta m_{15}(B) = 2.17 \pm 0.02$ mag (F09)[10]. Line velocities of SN 2008ha are as low as $\sim 2,000$ km s^{-1} around the maximum brightness (V09; F09). Thus, the ejecta is expected to have very low energy. V09 suggested that the ejecta mass is $M_{\rm ej} = 0.1 - 0.5\ M_\odot$ and the kinetic energy is $E_{\rm kin} = (1-5) \times 10^{49}$ erg, while F09 estimated $M_{\rm ej} = 0.15\ M_\odot$ and $E_{\rm kin} = 2.3 \times 10^{48}$ erg. The estimated mass of the ejected ^{56}Ni is also as small as $(3-5) \times 10^{-3}$ $M_\odot$ (V09) and $(3.0 \pm 0.9) \times 10^{-3}\ M_\odot$ (F09).

Given the low energy and the small mass of the ejecta as estimated from its spectral features and LC shape as well as its star-forming host galaxy, V09 concluded that SN 2008ha is not a thermonuclear explosion but a core-collapse SN with fallback. F09 also pointed out the possibility of the core-collapse origin but did not exclude the possibility of a thermonuclear explosion. Indeed, based on the earliest spectrum observed, Foley et al. (2010) suggested that SN 2008ha is related to a thermonuclear explosion. Alternatively, Pumo et al. (2009) related SN 2008ha to an electron capture SN (Nomoto 1984).

In this paper, we show that the properties of SN 2008ha can be explained well by a fallback SN model. We first perform numerical calculations of hydrodynamics and nucleosynthesis for several progenitor models. Then, we perform radiative transfer calculations to obtain the bolometric LCs and photospheric velocities of these models to compare them with the observations of SN 2008ha.

In Section 2, we introduce the pre-SN models. Methods used in our calculations of hydrodynamics, nucleosynthesis, and bolometric LCs are described in Section 3. We show our results of hydrodynamical calculations in Section 4. The results are compared with the observed bolometric LC and photospheric velocity of SN 2008ha in Section 5. Discussion and conclusions are given in Section 6.

2. PRESUPERNOVA MODELS

The spectra of SN 2008ha do not show hydrogen lines, which implies the progenitor of SN 2008ha has lost its H-rich envelope before the explosion. In addition, the identification of He lines in the spectra of SN 2008ha is very difficult because the lines are overcrowded (see the supplementary Figure 4 of V09 and Figure 8 of F09 for line identifications). Thus, both a helium star and a carbon + oxygen (CO) star are possible candidates for the progenitor of SN 2008ha.

We use pre-SN models of solar metallicity with main-sequence masses of 13 $M_\odot$, 25 $M_\odot$, and 40 $M_\odot$ calculated by Umeda & Nomoto (2002, 2005). As these models have a H-rich envelope, a He star is constructed by assuming that the whole H-rich envelope is lost either by stellar wind or Roche-lobe overflow of a close binary, and only the He core remains at the pre-SN stage. The boundary between the He core and the H-rich envelope is assumed to be at the location X(H)= 0.1 (hereafter, X(M) denotes the mass fraction of the element M). We adopt the 25 $M_\odot$ and 40 $M_\odot$ models to construct the He star models 25He and 40He, respectively. The He core masses of 25He and 40He are 7.0 $M_\odot$ and 15 $M_\odot$, respectively.

[10] $\Delta m_{15}(B)$ is the decline of the B band magnitude in 15 days since the B-band maximum.

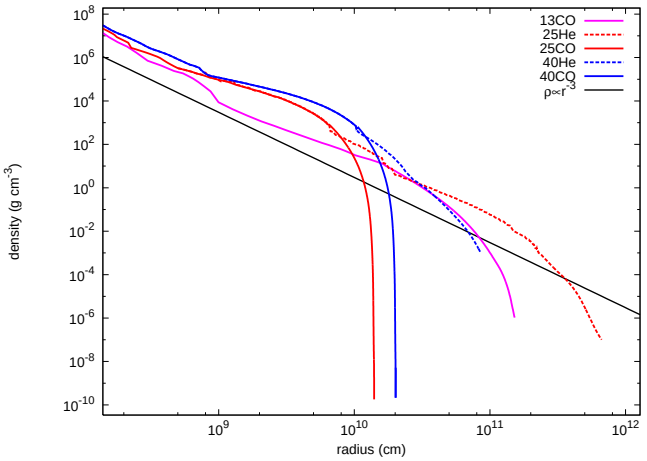

FIG. 1.— Density structure of the progenitor models. The line of $\rho \propto r^{-3}$ is also shown for comparison.

The CO star models are constructed by assuming that both the H-rich and He envelopes are lost and a CO core remains. The boundary between the He envelope and the CO core is set at X(He)= 0.1. We construct CO star models, 13CO, 25CO, and 40CO, from the 13 $M_\odot$, 25 $M_\odot$, and 40 $M_\odot$ models, respectively. The CO core masses of 13CO, 25CO and 40CO are 2.7 $M_\odot$, 5.7 $M_\odot$, and 14 $M_\odot$, respectively. The density structures of all the models used in this paper are shown in Figure 1.

3. METHODS

3.1. *Hydrodynamics and Nucleosynthesis*

Calculations of hydrodynamics and nucleosynthesis are performed by using a spherical Lagrangian hydrodynamic code with a piecewise parabolic method (Colella & Woodward 1984). The calculation of explosive nucleosynthesis is coupled with hydrodynamics and the adopted reaction network includes 13 α-particles, i.e., ^{4}He, ^{12}C, ^{16}O, ^{20}Ne, ^{24}Mg, ^{28}Si, ^{32}S, ^{36}Ar, ^{40}Ca, ^{44}Ti, ^{48}Cr, ^{52}Fe, and ^{56}Ni (see also Nakamura et al. 2001 for details). The main purpose of the nucleosynthesis calculations is to see how much ^{56}Ni is produced at the explosion. For this purpose, inclusion of only α-nuclei is a good approximation because α-nuclei are the predominant yields of SNe. The equation of state takes into account gas, radiation, Coulomb interactions between ions and electrons, $e^- - e^+$ pair (Sugimoto & Nomoto 1975), and phase transition (Nomoto 1982; Nomoto & Hashimoto 1988). To obtain many ($E_{\rm kin} - M_{\rm ej}$) relations, we compute several hydrodynamical models without following nucleosynthesis and including only gas and radiation in the equation of state. The omitted physics in the equation of state, such as Coulomb interaction, mainly affects the result of nucleosynthesis and does not have much effect on $E_{\rm kin}$ and $M_{\rm ej}$.

As the explosion mechanism of core-collapse SNe is not yet clear, we initiate the explosion as a thermal bomb (e.g., Nakamura et al. 2001). We put the thermal energy at $M_r = 1.4\ M_\odot$ in the nucleosynthesis calculations, assuming that the 1.4 $M_\odot$ neutron star is initially formed and the central remnant is treated as a point gravita-

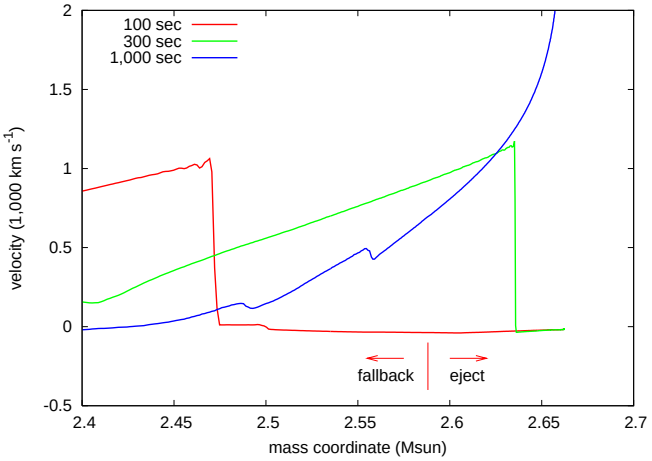

FIG. 2.— Change in the velocity profile shows the shock propagation for the hydrodynamical model 13CO_2. The time since the explosion is shown. The mass cut between the ejecta and the fallback material is determined by whether the point exceeds the escape velocity or not.

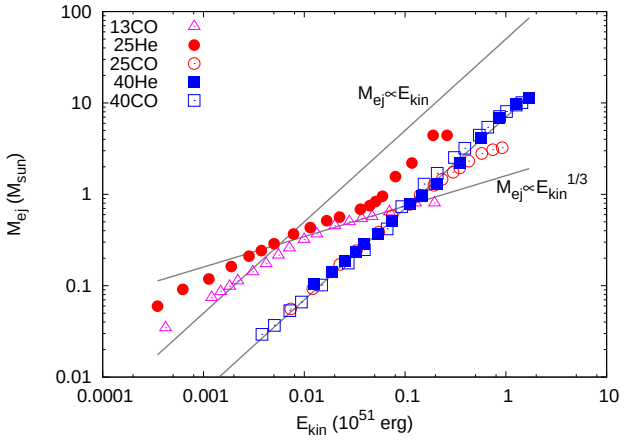

FIG. 3.— Results of hydrodynamical calculations in the diagram of the kinetic energy of the ejecta ($E_{\rm kin}$) and the ejecta mass ($M_{\rm ej}$). $E_{\rm kin}$ is the final kinetic energy at infinity. For comparison, the lines of $M_{\rm ej} \propto E_{\rm kin}$ and $M_{\rm ej} \propto E_{\rm kin}^{1/3}$ are also shown.

tional source. Here, M_r is the mass coordinate from the center. There exist several ways to induce SN explosions, e.g., a kinetic piston (e.g., Woosley & Weaver 1995), but it is suggested that the results of nucleosynthesis are not sensitive to how energy is injected (Aufderheide et al. 1991). However, note that Young & Fryer (2007) reports that the amount of fallback in low energy explosions depends on the method by which explosions are indeuced. Generally, explosions by kinetic piston have less fallback because they tend to create stronger shocks and thus, the difference in the method also affects the yields of the nucleosynthesis.

3.2. *Bolometric Light Curve*

Bolometric LCs are calculated by using an LTE radiative transfer code (Iwamoto et al. 2000). This code assumes a gray atmosphere for the γ-ray transport. For the optical radiation transport, electron scattering and line opacities are taken into account. Electron number density is evaluated by solving the Saha equation. For simplicity, the line opacity is assumed to be a constant 0.06 cm^2 g^{-1}. This value has been previously used for the explosion of CO stars (Maeda et al. 2003a). The gray γ-ray opacity is set to be 0.027 cm^2 g^{-1}, which is known to be a good approximation (Axelrod 1980). Positrons emitted by the decay of ^{56}Co are assumed to be trapped in situ. To compare with the computed bolometric LCs, the observed bolometric LC of SN 2008ha is constructed as shown in the Appendix.

4. RESULTS OF HYDRODYNAMICAL CALCULATIONS

4.1. $E_{\rm kin} - M_{\rm ej}$ *Relation*

We calculate the hydrodynamics of the explosions and fallback for 25He, 40He, 13CO, 25CO, and 40CO with various input energies. In Figure 2, the change in the velocity profile shows the propagation of the shock wave. When the explosion energy $E_{\rm kin}$ is low, the inner part of the progenitor cannot overcome the gravitational potential provided by the central remnant and thus falls back on to the remnant. In such cases, only the outer layers of the progenitor are ejected. The boundary between the fallback region and the ejecta is determined by whether the velocity of the region exceeds the escape velocity. We set a mass cut at this boundary to determine $M_{\rm ej}$. The expansion of the region above this mass cut eventually becomes homologous. These homologous models are used for the calculations of the bolometric LCs.

In Table 1, we summarize $E_{\rm kin}$ and $M_{\rm ej}$ for all our hydrodynamical models and plot them in Figure 3. All the models with fallback are found to be on the line of either $M_{\rm ej} \propto E_{\rm kin}$ or $M_{\rm ej} \propto E_{\rm kin}^{1/3}$. The reason why there exist two relations between $E_{\rm kin}$ and $M_{\rm ej}$ can be understood as due to a difference in the density structure. The density structure of the progenitor affects the manner of the shock propagation, thus leading to the difference in the $E_{\rm kin} - M_{\rm ej}$ relation.

Suppose the density structure of the progenitor is expressed as $\rho \propto r^{-\alpha}$, where ρ is the density and r is the radius. Sedov (1959) showed that a shock wave is accelerated when it is propagating along the density structure with $\alpha > 3$ while it decelerates when propagating along the density structure with $\alpha < 3$. This means that to achieve a certain velocity at a place with a density structure of $\alpha < 3$, more energy is required than the case of $\alpha > 3$. As the escape velocity determines the boundary between the ejecta and the fallback region, the boundary is expected to be closer to the central remnant for the case for $\alpha > 3$ than that of $\alpha < 3$ if the same energy is injected. Our hydrodynamical models show that if $\alpha > 3$ at the boundary between the ejecta and the fallback region, the results follow the relation $M_{\rm ej} \propto E_{\rm kin}$, and if $\alpha < 3$, they follow $M_{\rm ej} \propto E_{\rm kin}^{1/3}$. The exact physical reason why $M_{\rm ej}$ and $E_{\rm kin}$ are related as $M_{\rm ej} \propto E_{\rm kin}$ and $M_{\rm ej} \propto E_{\rm kin}^{1/3}$ is still unclear. We just treat it as an empirical relation in this paper and leave it as an open question.

Figure 4 (left) shows the density structure of the progenitor model 25He. In Figure 4 (right), we plot hydrodynamical models (Nos. 1-19) for 25He listed in Table 1. The numbers attached to the points in the left panel of the figure are the same model numbers as in the right panel. The location of the model points indicates the

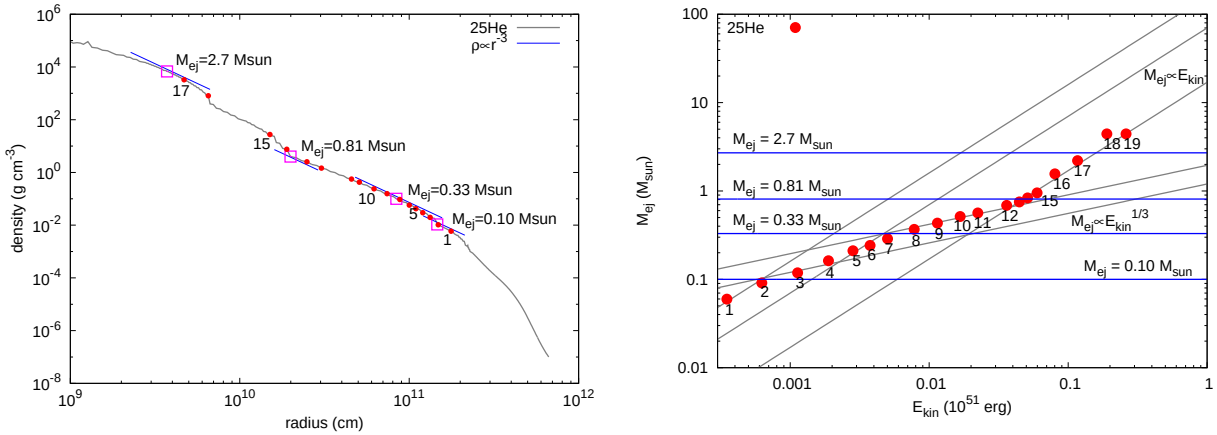

FIG. 4.— Density structure of 25He and the $E_{\rm kin} - M_{\rm ej}$ relation of 25He. Along the structure line, we plot the points where the density slope is $\rho \propto r^{-3}$ (open squares). In the right panel, we plot hydrodynamical models (Nos. 1-19) for 25He listed in Table 1. The numbers attached to the points in the left panel are the same model numbers as in the right panel. The location of the model points indicates the mass cut of the hydrodynamical model. Looking at the density structure from outside, there is a small region where the density structure follows $\alpha < 3$ which corresponds to model 3 with $M_{\rm ej} \simeq 0.10\ M_\odot$. Thus, the $E_{\rm kin} - M_{\rm ej}$ relation of the models around this region follows $M_{\rm ej} \propto E_{\rm kin}^{1/3}$. At $M_{\rm ej} \simeq 0.33 - 0.81\ M_\odot$, the corresponding models 8-13 have a density structure with $\alpha < 3$, thus following $M_{\rm ej} \propto E_{\rm kin}^{1/3}$. At larger $M_{\rm ej}$, models 14-17 have a density structure with $\alpha > 3$ and follow $M_{\rm ej} \propto E_{\rm kin}$. The last two models, 18 and 19, have no fallback.

TABLE 1
RESULTS OF HYDRODYNAMICAL CALCULATIONS

	13CO		25He		25CO		40He		40CO	
No.	$E_{\rm kin}$	$M_{\rm ej}$	$E_{\rm kin}$	$M_{\rm ej}$	$E_{\rm kin}$	$M_{\rm ej}$	$E_{\rm kin}$	$M_{\rm ej}$	$E_{\rm kin}$	$M_{\rm ej}$
1	0.00042	0.035	0.00035	0.060	0.0073	0.056	0.012	0.10	0.0038	0.029
2	0.0012	0.074	0.00062	0.091	0.012	0.093	0.019	0.14	0.0050	0.037
3	0.0015	0.086	0.0011	0.12	0.022	0.17	0.026	0.19	0.0072	0.053
4	0.0018	0.098	0.0019	0.16	0.033	0.24	0.033	0.23	0.0094	0.066
5	0.0022	0.11	0.0028	0.21	0.055	0.39	0.039	0.29	0.015	0.10
6	0.0031	0.14	0.0038	0.24	0.074	0.58	0.054	0.37	0.027	0.18
7	0.0042	0.17	0.0050	0.29	0.11	0.78	0.073	0.51	0.039	0.25
8	0.0055	0.22	0.0078	0.37	0.14	0.98	0.11	0.78	0.066	0.42
9	0.0071	0.26	0.011	0.43	0.19	1.3	0.15	0.95	0.093	0.73
10	0.010	0.32	0.017	0.51	0.23	1.5	0.21	1.2	0.15	1.3
11	0.013	0.37	0.022	0.56	0.30	1.7	0.35	2.2	0.21	1.7
12	0.020	0.45	0.036	0.69	0.35	1.9	0.56	4.1	0.31	2.5
13	0.028	0.50	0.045	0.75	0.43	2.7	0.86	6.8	0.39	3.2
14	0.037	0.54	0.051	0.83	0.58	2.8	1.3	9.7	0.54	4.4
15	0.047	0.57	0.060	0.95	0.74	3.1	1.7	11	0.66	5.4
16	0.070	0.64	0.080	1.6	0.92	3.2	...	...	0.87	7.1
17	...	...	0.12	2.2	...	...	...	...	1.0	8.1
18	...	...	0.19	4.4[a]	...	...	...	...	1.3	9.5
19	...	...	0.26	4.4[a]	...	...	...	...	1.4	10

NOTE. — The units of $E_{\rm kin}$ and $M_{\rm ej}$ are 10^{51} erg and $M_\odot$, respectively.
[a] No fallback

mass cut of the hydrodynamical model. Looking at the density structure from outside, there is a small region where the density structure follows $\alpha < 3$ which corresponds to model 3 with $M_{\rm ej} \simeq 0.10\ M_\odot$. Thus, the $E_{\rm kin} - M_{\rm ej}$ relation of the models around this region follows $M_{\rm ej} \propto E_{\rm kin}^{1/3}$. At $M_{\rm ej} \simeq 0.33 - 0.81\ M_\odot$, the corresponding models 8-13 have a density structure with $\alpha < 3$, thus following $M_{\rm ej} \propto E_{\rm kin}^{1/3}$. At larger $M_{\rm ej}$, models 14-17 have a density structure with $\alpha > 3$ and follow $M_{\rm ej} \propto E_{\rm kin}$. The last two models, 18 and 19, have no fallback.

For the extremely low $E_{\rm kin}$, the mass cut in the explosion models lies in the outermost layer where the density declines exponentially in all the progenitor models. Thus, the model sequences follow the relation $E_{\rm kin} \propto M_{\rm ej}$ at the low $E_{\rm kin}$ limit in the $E_{\rm kin} - M_{\rm ej}$ plane. This proportionality between $E_{\rm kin}$ and $M_{\rm ej}$ was also shown by Nadezhin & Frank-Kamenetskii (1963) in the context of nova explosions. Thus, the ejecta velocity, which is scaled as $v \propto (E_{\rm kin}/M_{\rm ej})^{1/2}$, would be a constant, being independent of $E_{\rm kin}$ for each progenitor model. This means that however low $E_{\rm kin}$ is, the ejecta velocity, i.e., the line velocities of the spectra, does not become lower than a certain asymptotic value.

4.2. *Rise Time - Ejecta Velocity Relation*

Based on the $E_{\rm kin} - M_{\rm ej}$ relation, we can construct a relation between observable quantities: the rise time (τ) of the LC versus velocity (v) of the ejecta. The ejecta velocity approximates the line velocities in the observed spectra. For each set of ($E_{\rm kin}$, $M_{\rm ej}$), τ is derived from the relation $\tau \propto \kappa^{1/2}(M_{\rm ej}^3/E_{\rm kin})^{1/4}$ (Arnett 1982), where κ is the

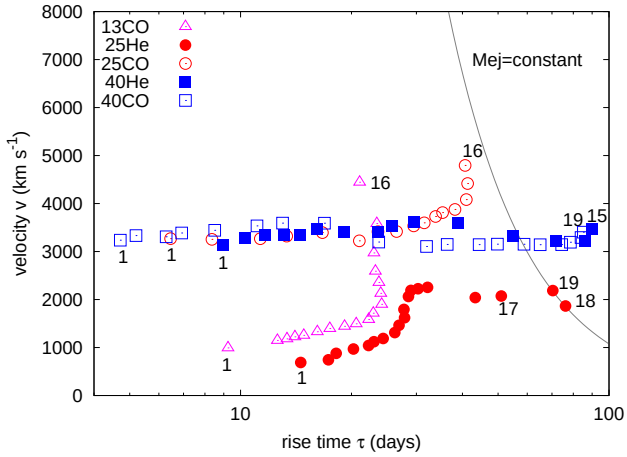

FIG. 5.— Results of hydrodynamical calculations in the diagram of the rise time (τ) and the ejecta velocity (v) defined by Equations (1) and (2). The attached numbers correspond to the numbers of the models shown in Table 1. The line on the right-hand side is the line $M_{\rm ej}$ = constant.

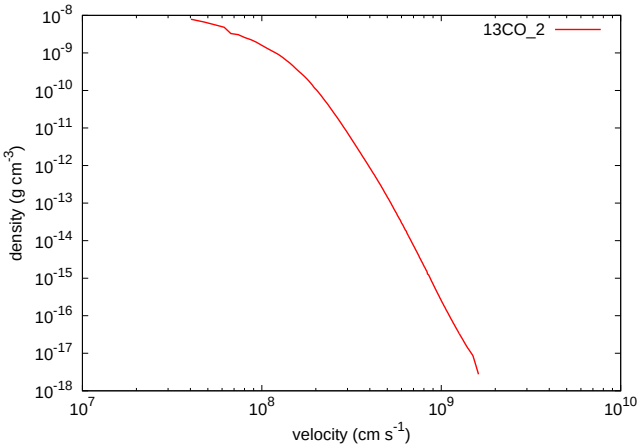

FIG. 6.— Density structures of 13CO_2 at 2 days after the explosion.

total opacity and v is simply scaled as $v \propto (E_{\rm kin}/M_{\rm ej})^{1/2}$. For simplicity, we assume that κ is constant for all the models. For illustration, we choose the proportional constants in τ and v to match the typical values of Type Ia SNe, $E_{\rm kin} = 1.4 \times 10^{51}$ erg, $M_{\rm ej} = 1.4\ M_\odot$, $\tau = 19.5$ days, and $v = 9000$ km s^{-1}, and get the relations:

$$\tau = 16.5 \left(\frac{(M_{\rm ej}/M_\odot)^3}{E_{\rm kin}/10^{51}{\rm erg}} \right)^{1/4} \quad {\rm days}, \qquad (1)$$

$$v = 9000 \left(\frac{E_{\rm kin}/10^{51}{\rm erg}}{M_{\rm ej}/M_\odot} \right)^{1/2} \quad {\rm km\ s^{-1}}. \qquad (2)$$

In Figure 5 we plot (τ, v) for the model sequences in Table 1 and Figure 3. As derived from Equations (1) and (2), the models with $M_{\rm ej} \propto E_{\rm kin}$ are located along the line with $\tau \propto M_{\rm ej}^{1/2} \propto E_{\rm kin}^{1/2}$ and $v \simeq$ constant, while the models with $M_{\rm ej} \propto E_{\rm kin}^{1/3}$ are located along the line with $\tau \simeq$ constant and $v \propto M_{\rm ej} \propto E_{\rm kin}^{1/3}$. For large $E_{\rm kin}$, all materials outside the proto-neutron star are ejected without fallback and $M_{\rm ej} = M_{\rm pro} - M_{\rm rem}$ is a constant, where $M_{\rm pro}$ is the progenitor's pre-SN mass and $M_{\rm rem}$ is the mass of the central remnant below the mass cut. As $M_{\rm ej}$ is a constant, τ and v follow the curve $\tau^2 v \propto M_{\rm ej}$ = constant, as derived from Equations (1) and (2). The black curve on the right side of Figure 5 shows the curve of $M_{\rm ej}$ = constant for model 25He.

Our hydrodynamical models have a wide range of τ as seen in Figure 5 and it implies that fallback SNe have a variety of LCs. However, v has only limited values for each progenitor and the progenitor of a fallback SN can be constrained not by its LC but by its photospheric velocity. In the next section, we constrain the progenitor of SN 2008ha mainly by using its photospheric velocity. As the observed line velocities around the maximum luminosity of SN 2008ha are $\sim$ 2000 km s^{-1}, it is expected that 25CO, 40He, and 40CO would have too high photospheric velocities (v) to be consistent with those of SN 2008ha.

5. SN 2008HA

We calculate bolometric LCs and the photospheric velocities for the models shown in Figure 3. We adopt the structure of the ejecta when it reaches the homologous expansion in hydrodynamical calculations and assume that ^{56}Ni is uniformly mixed throughout the ejecta. Among all the models shown in Figure 3, we find that model 13CO_2 with $(E_{\rm kin}, M_{\rm ej}) = (1.2 \times 10^{48}$ erg, $0.074\ M_\odot)$ is consistent with both the bolometric LC and the photospheric velocity of SN 2008ha. Fallback occurs in 13CO_2 and only the outermost layer of the progenitor is ejected. The density structure of the model is shown in Figure 6. Figure 7 shows that the calculated bolometric LC of 13CO_2 is in good agreement with the observed bolometric LC of SN 2008ha (see the Appendix). The ^{56}Ni mass ejected is assumed to be 0.003 $M_\odot$. The rise time of 13CO_2 is 9.8 days. LCs from other explosion models of 13CO are also shown for comparison in Figure 7.

In the nucleosynthesis calculation, the explosion of 13CO_2 produces 0.15 $M_\odot$ of ^{56}Ni at $M_r > 1.4\ M_\odot$. If we assume uniform mixing of ^{56}Ni at $M_r > 1.4\ M_\odot$, the ejecta will contain 0.0086 $M_\odot$ ^{56}Ni (Table 2). To reproduce the luminosity of SN 2008ha, 0.003 $M_\odot$ of ^{56}Ni needs to be contained in the ejecta. This implies that mixing due to the Rayleigh-Taylor instability (e.g., Hachisu et al. 1991; Joggerst et al. 2009) or a jet (e.g., Maeda & Nomoto 2003b; Tominaga 2009) occurs in SN 2008ha to bring ^{56}Ni to the outermost layer before the fallback.

Figure 8 shows the photospheric velocities of 13CO_2 compared with the observed line velocities of SN 2008ha (Figure 5 of F09). Among the line velocities shown in F09, we take Na I D and O I 7774 as good tracers of the photospheric velocity because these lines can be clearly distinguished and their line velocities are slower than other lines. The evolution of the photospheric velocity of 13CO_2 follows the line velocities of these tracers well. Thus, it is expected that our models will also be consistent with the observed spectra of SN 2008ha. Detailed synthetic spectra based on our model will be shown in a forthcoming paper (D. N. Sauer et al. 2010, in preparation).

TABLE 2
Uniform Composition Based on the Result of the Nucleosynthesis of 13CO_2

^{4}He	^{12}C	^{16}O	^{20}Ne	^{24}Mg	^{28}Si	^{32}S	^{36}Ar	^{40}Ca	^{44}Ti	^{48}Cr	^{52}Fe	^{56}Ni
0.037	0.20	0.32	0.14	0.066	0.063	0.034	0.0065	0.0045	0.00051	0.0017	0.011	0.12

Note. — The mass fraction of each element is shown.

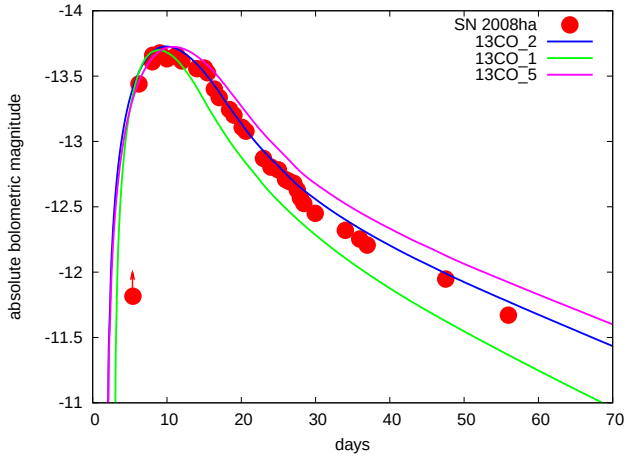

Fig. 7.— Bolometric LC of SN 2008ha and the calculated bolometric LCs for some explosion models of 13CO are shown. The bolometric LC of SN 2008ha is constructed as explained in the Appendix. Horizontal axis represents days since the explosion of the theoretical LCs of 13CO_2 and 13CO_5. The explosion date of 13CO_1 is + 1 day in the figure. The kinetic energy and mass of ejecta of 13CO_2 are $E_{\rm kin} = 1.2 \times 10^{48}$ erg and $M_{\rm ej} = 0.074\ M_{\odot}$. The mass of ^{56}Ni is 0.003 $M_{\odot}$ in 13CO_2. The rise time of 13CO_2 is 9.8 days. $E_{\rm kin}$ and $M_{\rm ej}$ of 13CO_1 and 13CO_5 are $(E_{\rm kin},\ M_{\rm ej}) = (4.2\times10^{47}{\rm erg}, 0.035 M_{\odot})$ and $(2.2\times10^{48}{\rm erg}, 0.11 M_{\odot})$, respectively.

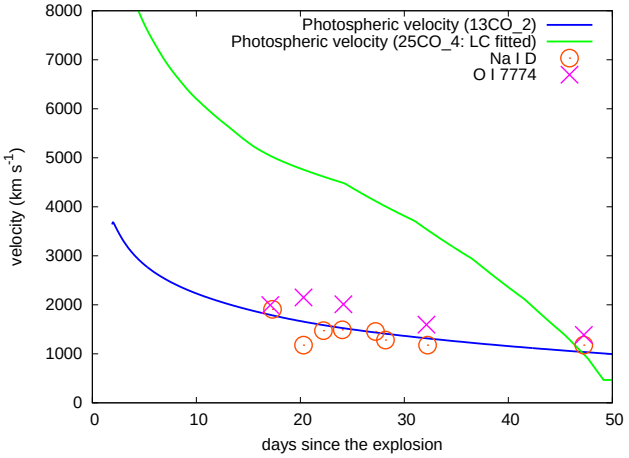

Fig. 8.— Photospheric velocities of 13CO_2 obtained from the bolometric LC calculations. These are compared with the observed line velocities of Na I D and O I 7774 from Figure 5 of F09, which are expected to be good tracers of the photosphere. Days are measured since the explosion date of each model. The rise time of 13CO_2 is 9.8 days. We also show the explosion model of 25CO which has $E_{\rm kin} = 3.3\times10^{49}$ erg and $M_{\rm ej} = 0.24\ M_{\odot}$. This model reproduces well the LC of SN 2008ha but the photospheric velocity is too high to be comparable to the line velocities of SN 2008ha.

The model from 25CO whose photospheric velocity is shown in Figure 8 has $E_{\rm kin} = 3.3 \times 10^{49}$ erg and $M_{\rm ej}$ = 0.24 $M_{\odot}$ (25CO_4). This model reproduce well the bolometric LC of SN 2008ha. However, the photospheric velocity of this model is much higher than the line velocities of SN 2008ha. This result is expected from Figure 5 because the ejecta velocities (v) of the explosion models of 25CO are too high for SN 2008ha (Figure 5). On the other hand, the explosion model of 25He with the smallest energy we calculated ($E_{\rm kin} = 3.5 \times 10^{47}$ erg) still has a long rise time compared to SN 2008ha. Its LC is close to that of the explosion model 13CO_5 shown in Figure 7, which has almost the same τ (Figure 5). It is expected from Figures 3 and 5 that an explosion model of 25He with smaller energy could be consistent with SN 2008ha but the energy will have to be quite small ($E_{\rm kin} \simeq 10^{47}$ erg). Still, there remains a possibility that such an SN with a very small explosion energy could emerge as a result of the fallback.

Although we assume a large amount of mass loss during the evolution of the progenitors, we do not assume the existence of a circumstellar matters due to a mass loss in our LC calculations. If the circumstellar matters are dense enough, SNe with fallback will be brightened by the interaction between the ejecta of SNe and the circumstellar matters (Fryer et al. 2009). According to Fryer et al. (2009), this interaction could result in SNe having LCs with rising times and luminosities similar to those of SN 2008ha. Considering the fact that we do not see any evidence for the interaction in the spectra of SN 2008ha and there is no sudden drop in the tail of the LC of SN 2008ha, which is expected in the interaction-powered SN models and is naturally explained by the nuclear decay of ^{56}Co, we think that SN 2008ha is likely to be powered by the nuclear decay of ^{56}Ni and the circumstellar matter around the progenitor of SN 2008ha is so thin that the interaction does not become the major energy source of the LC. However, in conditions such as the mixing of the whole exploding star does not occur, almost all ^{56}Ni would fall back to the central remnant and only the interaction between the ejecta and the circumstellar matter would be the energy source to brighten the SN. We still do not have a clear observational SN with fallback brightened by the interaction, but such SNe might be discovered in the future.

6. DISCUSSION AND CONCLUSIONS

We have found a fallback SN model (13CO_2) whose bolometric LC and photospheric velocity are both in good agreement with the observations of SN 2008ha. The ejecta of the model has very low explosion energies and ejecta masses: $(E_{\rm kin},\ M_{\rm ej}) = (1.2 \times 10^{48}$ erg, 0.074 $M_{\odot})$. The explosion models from the progenitors of 25CO, 40CO and 40He are not in agreement with the observations of SN 2008ha because the photospheric velocities of these models are too high to be compatible with the observed line velocities of SN 2008ha (Figure 5). One might think that a model with sufficiently small $E_{\rm kin}$ can have a low photospheric velocity. However, as shown in Figure 3, smaller $E_{\rm kin}$ leads to a larger fallback and thus smaller $M_{\rm ej}$ as $M_{\rm ej} \propto E_{\rm kin}$. In this case, the ve-

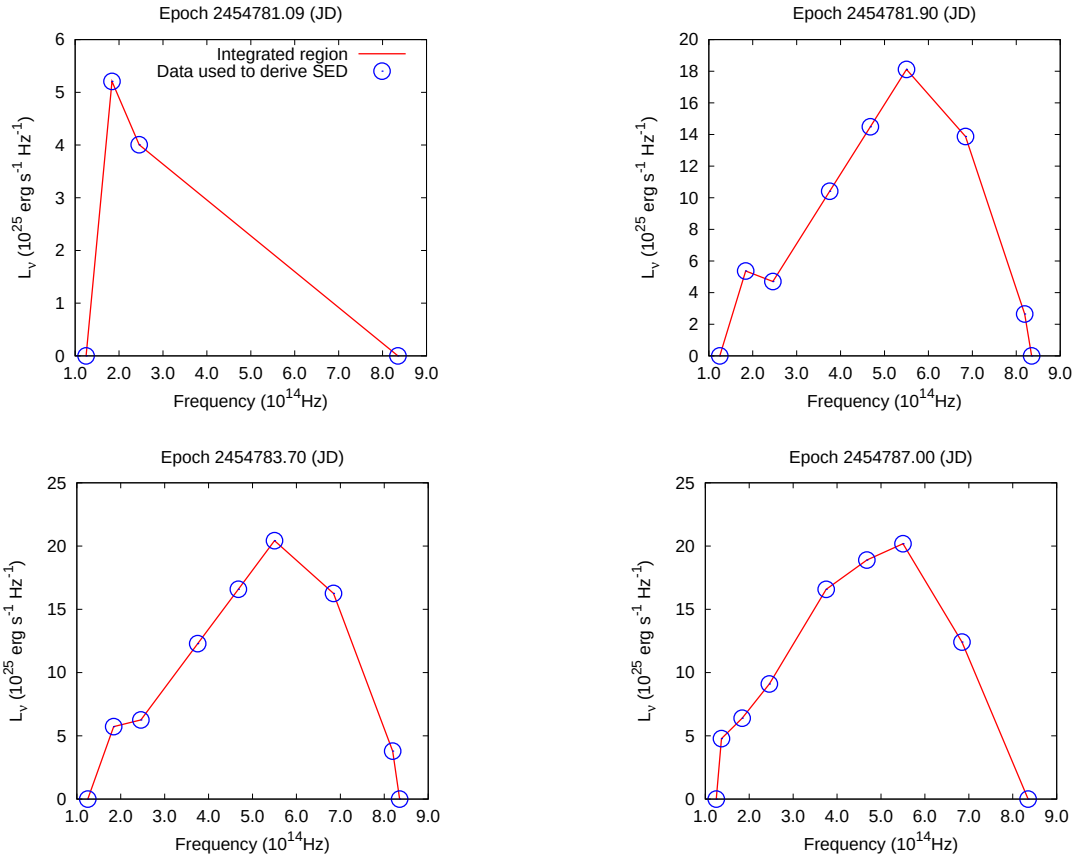

FIG. 9.— Samples of the SED to construct the bolometric LC. The top left SED corresponds to the first point of the bolometric LC. Linear interpolations are made to fill the gaps in observations. The details of the interpolation are described in the Appendix.

locity of the ejecta, $v \propto (E_{\rm kin}/M_{\rm ej})^{1/2}$, will not become smaller. Alternatively, the explosion of 25He requires $E_{\rm kin} \simeq 10^{47}$ erg to have a rise time similar to SN 2008ha.

The difference between the successful and the unsuccessful progenitor models to explain SN 2008ha stems from the difference in the density structure. As discussed in Section 4.1, the density structure affects the propagation of the shock wave and thus the relation between $E_{\rm kin}$ and $M_{\rm ej}$. This means that whether a model can have the appropriate $(E_{\rm kin}, M_{\rm ej})$ for SN 2008ha mainly depends on the density structure of the progenitor and not on the progenitor mass. Thus, the main-sequence mass of SN 2008ha cannot be constrained only by hydrodynamical calculations and 13CO would not be a unique progenitor candidate for SN 2008ha. Other progenitor models with appropriate density structures are also expected to reproduce the observational properties of SN 2008ha.

The fact that faint SNe like SN 2008ha could emerge from the fallback of massive stars is also related to long gamma-ray bursts (LGRBs) without accompanied SNe (see also V09). LGRBs are thought to result from the death of massive stars and the fact that nearby LGRBs are accompanied by bright SNe (e.g., GRB 030329 and SN 2003dh, Hjorth et al. 2003; GRB 100316D and SN 2010bh, Chornock et al. 2010) is one of the evidence for the scenario that relates LGRBs to the death of massive stars. However, some LGRBs are not accompanied by SNe even though they are close enough to be observed (e.g., GRB 060614 (Gehrels et al. 2006; Fynbo et al. 2006; Della Valle et al. 2006; Gal-Yam et al. 2006)) and this is one of the challenging problems of the theory of LGRBs. Several scenarios are proposed, e.g., a neutron star-white dwarf merger (e.g., King et al. 2007) and a massive stellar death with a faint/dark SN (e.g., Tominaga et al. 2007). In this paper, we show that core-collapse SNe with fallback can be very faint and reproduce the observations of a faint SN (SN 2008ha). This supports the scenario that LGRBs without observed bright SNe are accompanied by very faint SNe with fallback. In fact, theories of LGRBs like the collapsar model (Woosley 1993) assume black hole formation with an accretion disk and this picture is consistent with our fallback SN model in the sense that most part of progenitors accretes to the central remnant and the central remnant becomes massive enough to be a black hole. This process could induce an LGRB, and it is possible that an LGRB was actually associated with SN 2008ha. We could have missed the LGRB because the jet of the LGRB was not directed to the Earth. In addition, our fallback SN model for SN 2008ha requires some mixing process to provide the ejecta with ^{56}Ni and the jet from the LGRB could have played a role in the mixing.

Currently, several SNe are reported to have features similar to SN 2008ha. SN 2005E is one of the examples (Perets et al. 2010; see also Figure 7 of F09). As SN 2005E is found far from the disk of the host galaxy, SN 2005E is unlikely to be a core-collapse SN. However, its spectra do not show the characteristics of thermonuclear

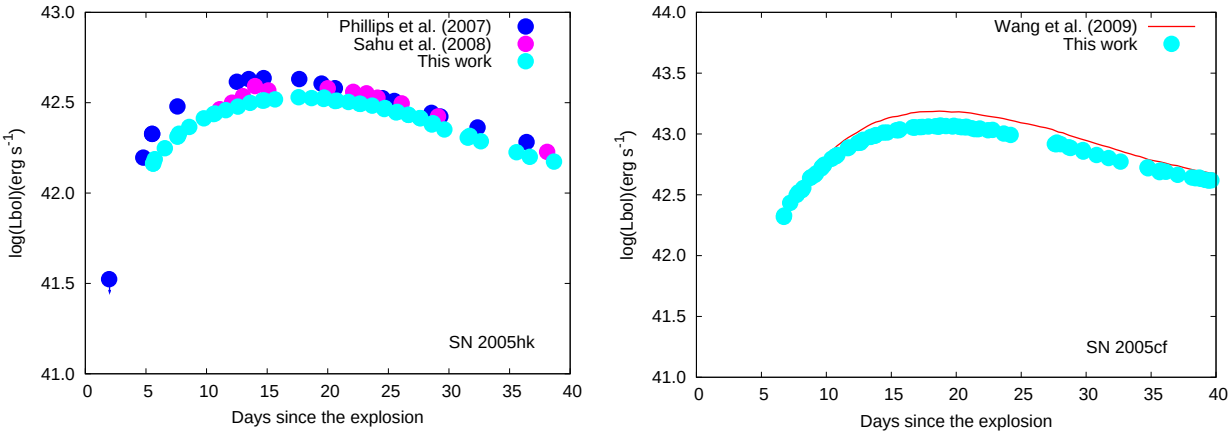

FIG. 10.— Comparison of the bolometric LCs with those obtained in previous works. We apply our method to another SN 2002cx-like supernova SN 2005hk (Phillips et al. 2007, Sahu et al. 2008) and a normal Type Ia supernova SN 2005cf (Wang et al. 2009). The rise times of SN 2005hk and SN 2005cf are assumed to be 15 days (Phillips et al. 2007) and 18 days (Wang et al. 2009), respectively. Our bolometric LCs tend to be a bit fainter around the maximum epoch but the decline rate and the luminosity at later epochs are in good agreement with other bolometric LCs obtained in previous works.

explosions. Thus, SN 2005E is suggested to be a new type of stellar explosion (Perets et al. 2010). Perets et al. (2010) showed that the late phase spectra of SN 2005E contain strong emission lines of [Ca II] $\lambda\lambda$7291, 7323 and suggested that those are the results of Ca enrichment in the ejecta. As this feature is similar to SN 2008ha (Figure 7 of F09), they suggested that SN 2005E is related to SN 2008ha. However, the line velocities of SN 2008ha (~ 2000 km s^{-1}) are considerably slower than SN 2005E ($\sim 11,000$ km s^{-1}). Thus, it is not so obvious that SN 2005E has the same origin as SN 2008ha. Kawabata et al. (2010) reported that Type Ib SN 2005cz is another example of an SN that shows prominent Ca emissions and they related it to the core-collapse SN from a low mass ($\simeq 10\ M_\odot$) star. In this paper, we suggest that SN 2008ha is of core-collapse origin. Other SN 2002cx-like SNe, SN 2002cx (Li et al. 2003; Jha et al. 2006) and SN 2005hk (Phillips et al. 2007; Sahu et al. 2008), are considered to be weak thermonuclear explosions while SN 2005E seems to be neither a core-collapse nor a typical thermonuclear explosion (Perets et al. 2010). Thus, SN 2002cx-like SNe might contain SNe with several kinds of origins and other criteria to classify them might be required. We need more samples of SN 2002cx-like SNe to clarify such criteria. See the supplementary information of Kawabata et al. (2010) for more intensive discussion for these Ca-rich SNe.

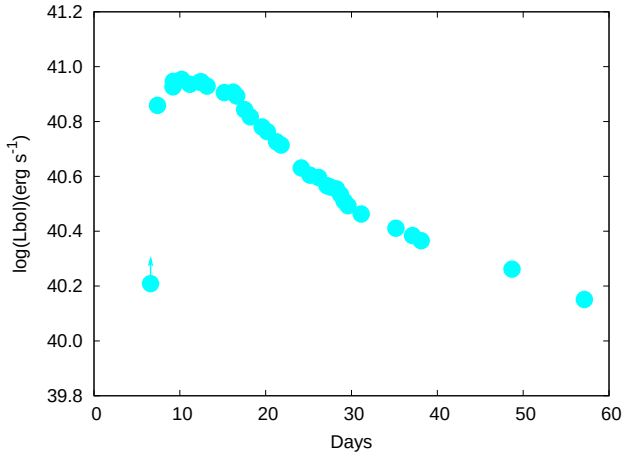

FIG. 11.— Obtained bolometric LC of SN 2008ha. The rise time is set to 10 days in this plot.

We propose that SN 2008ha can be a core-collapse SN with fallback. However, it is not obvious that the features of the intermediate-mass elements that appeared in the earliest spectrum of SN 2008ha (Foley et al. 2010) can be synthesized by our model and this will be investigated in a forthcoming paper (D. N. Sauer et al. 2010, in preparation). Our model does not exclude the possibility that SN 2008ha is a thermonuclear explosion. However, simple estimates of $M_{\rm ej}$ by V09 and F09 are far below the Chandrasekhar mass limit ($1.4\ M_\odot$), which is required to ignite a thermonuclear explosion of a white dwarf. However, these estimates assume that the total opacity κ is constant. It is possible that the effects of the opacity are large enough to create the appearance of a thermonuclear explosion similar to SN 2008ha. If this is the case, the opacity must become very low to match the fast rise of SN 2008ha as expected from the relation $\tau \propto \kappa^{1/2}(M_{\rm ej}^3/E_{\rm kin})^{1/4}$. Other kinds of explosions such as 'Ia' SNe (e.g., Shen et al. 2010) or accretion-induced collapses (e.g., Darbha et al. 2010) might also be candidates but there still do not exist sufficient models that are consistent with SN 2008ha.

We thank Sergei I. Blinnikov for useful discussions and comments. Numerical calculations and data analysis were in part carried out on the general-purpose PC farm at Center for Computational Astrophysics, CfCA, of National Astronomical Observatory of Japan. This research has been supported in part by World Premier International Research Center Initiative, MEXT, and by the Grant-in-Aid for Scientific Research of the JSPS (20540226, 20840007, 21840055) and MEXT (19047004, 22012003), Japan.

APPENDIX

CONSTRUCTION OF BOLOMETRIC LIGHT CURVE

We construct the bolometric LC of SN 2008ha by using the $UBVRIJHK$ band LCs presented by F09. For each epoch, we derive the spectral energy distribution (SED) and obtain the bolometric luminosity by integrating the SED. To estimate the absolute magnitude of each band, we use the distance modulus $\mu = 31.64$ mag and the color excess $E(B-V) = 0.08$ mag (F09). Reddening is corrected by following Cardelli et al. (1989). For each epoch, we use the observational data if they are available. If there is no observation of a band at a certain epoch, we deduce the magnitude of the band by linearly interpolating the observed magnitude of the nearest epochs. If no observational data are available before or after the observation as in the first few epochs when no RIK band data are available, we linearly interpolate data points on the SED. Finally, we integrate the SED by constructing trapezoids and triangles by connecting the $UBVRIJHK$ data and the two edges. The two edges are chosen to be 1.25×10^{14} Hz and 8.35×10^{14} Hz, close to the frequencies of the K band and U band. Some samples of the SED are shown in Figure 9. We calculate the bolometric LCs of SN 2005hk (Phillips et al. 2007, Sahu et al. 2008) and SN 2005cf (Wang et al. 2009) to check our method (Figure 10). Our bolometric LCs are in a good agreement with the bolometric LCs obtained in the previous studies.

The bolometric LC of SN 2008ha obtained by our method is shown in Figure 11. As the first point is constructed by only the JH data, we assume that the actual luminosity at this epoch is higher. The rise time of our bolometric LC is consistent with that of the quasi-bolometric LC constructed by F09.

REFERENCES

Arnett, W. D. 1982, ApJ, 253, 785
Aufderheide, M. B., Baron, E., & Thielemann, T.-K. 1991, ApJ, 370, 630
Axelrod, T. S. 1980, Ph.D. thesis, Univ. California, Santa Cruz
Branch, D., Baron, E., Thomas, R. C., Kasen, D., Li, W., & Filippenko, A. V. 2004, PASP, 116, 903
Bruenn, S. W., Mezzacappa, A., Hix, W. R., Blondin, J. M., Marronetti, P., Messer, O. E. B., Dirk, C. J., & Yoshida, S. 2009, American Institute of Physics Conference Series, 1111, 593
Burrows, A., Dessart, L., Ott, C. D., & Livne, E. 2007, Phys. Rep., 442, 23
Cardelli, J. A., Clayton, G. C., & Mathis, J. S. 1989, ApJ, 345, 245
Chevalier, R. A. 1989, ApJ, 346, 847
Chornock, R., et al. 2010, arXiv:1004.2262
Colella, P., & Woodward, P. R. 1984, J. Comput. Phy., 54, 174
Colgate, S. A. 1971, ApJ, 163, 221
Darbha, S., et al. 2010, arXiv:1005.1081
Della Valle, M., et al. 2006, Nature, 444, 1050
Foley, R. J., Brown, P. J., Rest, A., Challis, P. J., Kirshner, R. P., & Wood-Vasey, W. M. 2010, ApJ, 708, L61
Foley, R. J., et al. 2009, AJ, 138, 376 (F09)
Fryer, C. L. 1999, ApJ, 522, 413
Fryer, C. L., Hungerford, A. L., & Young, P. A. 2007, ApJ, 662, L55
Fryer, C. L., et al. 2009, ApJ, 707, 193
Fynbo, J. P. U., et al. 2006, Nature, 444, 1047
Gal-Yam, A., et al. 2006, Nature, 444, 1053
Gehrels, N., et al. 2006, Nature, 444, 1044
Hachisu, I., et al. 1991, ApJ, 368, 27
Hjorth, J., et al. 2003, Nature, 423, 847
Iwamoto, N., Umeda, H., Tominaga, N., Nomoto, K., & Maeda, K. 2005, Science, 309, 451
Iwamoto, K., et al. 2000, ApJ, 534, 660
Janka, H.-Th., Langanke, K., Marek, A., Martínez-Pinedo, G., & Müller, B. 2007, Phys. Rep., 442, 38
Jha, S., et al. 2006, AJ, 132, 189
Joggerst, C. C., Woosley, S. E., & Heger, A. 2009, ApJ, 693, 1780
Kawabata, K. S., et al. 2010, Nature, 465, 326
King, A., Olsson, E., & Davies, M. B. 2007, MNRAS, 374, L34
Li, W., et al. 2003, PASP, 115, 453
MacFadyen, A. I., Woosley, S. E., & Heger, A. 2001, ApJ, 550, 410
Maeda, K., Mazzali, P. A., Deng, J., Nomoto, K., Yoshii, Y., Tomita, H., & Kobayashi, Y. 2003a, ApJ, 593, 931
Maeda, K., & Nomoto, K. 2003b, ApJ, 598, 1163
Nadezhin, D. K., & Frank-Kamenetskii, D. A. 1963, Soviet Astro.-AJ, 6, 779
Nakamura, T., et al. 2001, ApJ, 555, 880
Nomoto, K. 1982, ApJ, 253, 798
Nomoto, K. 1984, ApJ, 277, 791
Nomoto, K., & Hashimoto, M. 1988, Phys. Rep., 163, 13
Perets, H. B., et al. 2010, Nature, 465, 322
Phillips, M. M., et al. 2007, PASP, 119, 360
Puckett, T., Moore, C., Newton, J., & Orff, T. 2008, Central Bureau Electronic Telegrams, 1567, 1
Pumo, M. L., et al. 2009, ApJ, 705, L138
Sahu, D. K., Tanaka, M., Anupama, G. C., Kawabata, K. S., Maeda, K., Tominaga, N., Nomoto, K., Mazzali, P. A., & Prabhu, T. P. 2008, ApJ, 680, 580
Sedov, L. 1959, Similarity and Dimensional Methods in Mechanics (New York: Academic)
Shen, K. J., Kasen, D., Weinberg, N. N., Bildsten, L., & Scannapieco, E. 2010, ApJ, 715, 767
Sugimoto, D., & Nomoto, K. 1975, Sci. Pap. Coll. Gen. Duc. Univ. Tokyo, 25, 109
Suwa, Y., Kotake, K., Takiwaki, T., Whitehouse, S. C., Liebendoerfer, M., & Sato, K. 2009, arXiv:0912.1157
Tominaga, N. 2009, ApJ, 690, 526
Tominaga, N., Maeda, K., Umeda, H., Nomoto, K., Tanaka, M., Iwamoto, N., Suzuki, T., & Mazzali, P. A. 2007, ApJ, 657, L77
Umeda, H., & Nomoto, K. 2002, ApJ, 565, 385
Umeda, H., & Nomoto, K. 2005, ApJ, 619, 427
Valenti, S., et al. 2009, Nature, 459, 674 (V09)
Wang, X., et al. 2009, ApJ, 697, 380
Woosley, S. E. 1993, ApJ, 405, 273
Woosley, S. E., & Weaver, T. A. 1995, ApJS, 101, 181
Young, A. P., & Fryer, C. L. 2007, ApJ, 664, 1033
Zhang, W., Woosley, S. E., & Heger, A. 2008, ApJ, 679, 639